Non-monotonic Velocity Dependence of Atomic Friction Induced by Multiple-Slips

Yiming Song[#,1,*] Jin Wang[#,2] Antoine Hinaut,[1] Sebastian Scherb,[1]

Shuyu Huang,[1,3] Thilo Glatzel,[1] Erio Tosatti,[2,4,5,†] and Ernst Meyer[1,‡]

[1]*Department of Physics, University of Basel, 4056 Basel, Switzerland*

[2]*International School for Advanced Studies (SISSA), 34136 Trieste, Italy*

[3]*Key Laboratory for Design and Manufacture of Micro-Nano Biomedical Instruments,*

School of Mechanical Engineering, Southeast University, 211189 Nanjing, China

[4]*CNR-IOM, Consiglio Nazionale delle Ricerche - Istituto*

Officina dei Materiali, c/o SISSA, 34136, Trieste, Italy

[5]*The Abdus Salam International Centre for Theoretical Physics (ICTP), 34151 Trieste, Italy*

(Dated: May 17, 2024)

Abstract

The transition from single to multiple atomic slips, theoretically expected and important in atomic-scale friction, has never been demonstrated experimentally as a function of velocity. Here we show by high-resolution friction force microscopy on monolayer MoS_2/ Au(111) that multiple-slips leave a unique footprint – a frictional velocity weakening. Specifically, in a wide velocity interval from 10 to 100 nm/s, friction surprisingly decreases. Model simulations show a similar non-monotonic behaviour at velocities in quantitative agreement with experiment. Results suggest a velocity-corrugation phase diagram, whose validity is proposed more generally.

In recent decades, the fundamental understanding of atomic stick-slip friction has been substantially improved by experimental tools, such as the atomic force microscope (AFM) [1–5]. The physics of a single nanoscale asperity sticking and sliding on a well-defined periodic substrate can be theoretically described and studied within the framework of the Prandtl-Tomlinson (PT) model [6, 7]. One of the most intriguing predictions of the PT model including thermal activation and reaction rate theory is that the friction force increases logarithmically with sliding velocity, which is different from both the Amontons-Coulomb and viscous friction laws [8–11]. A variety of experimental AFM measurements confirmed this logarithmic frictional growth, which spans many velocity ranges and has been validated on a variety of substrates, including ionic crystals [8], metals [10] and two dimensional materials [12]. Although thermally activated stick-slip sliding has also been exemplified by more advanced molecular dynamics simulations [10, 11], the PT model remains a fundamental and robust method for describing nanotribology [13].

One peculiar feature that the PT model also predicts for stick-slip sliding is the occurrence of multiple-slips once the velocity or load exceeds certain thresholds [14–16]. However, despite these predictions, multiple-slips have been found experimentally only for increasing loads [17, 18], but not as a function of velocity.

In this study a non-monotonic velocity dependence of atomic friction is observed during sliding of an AFM tip on a pristine MoS_2 surface, a system known for its ultra-low friction and wear-inhibiting properties [19, 20]. A PT-type model simulation plus analytical understanding demonstrates the atomic multiple-slips mechanism behind this non-monotonic

* yiming.song@unibas.ch

† tosatti@sissa.it

‡ ernst.meyer@unibas.ch

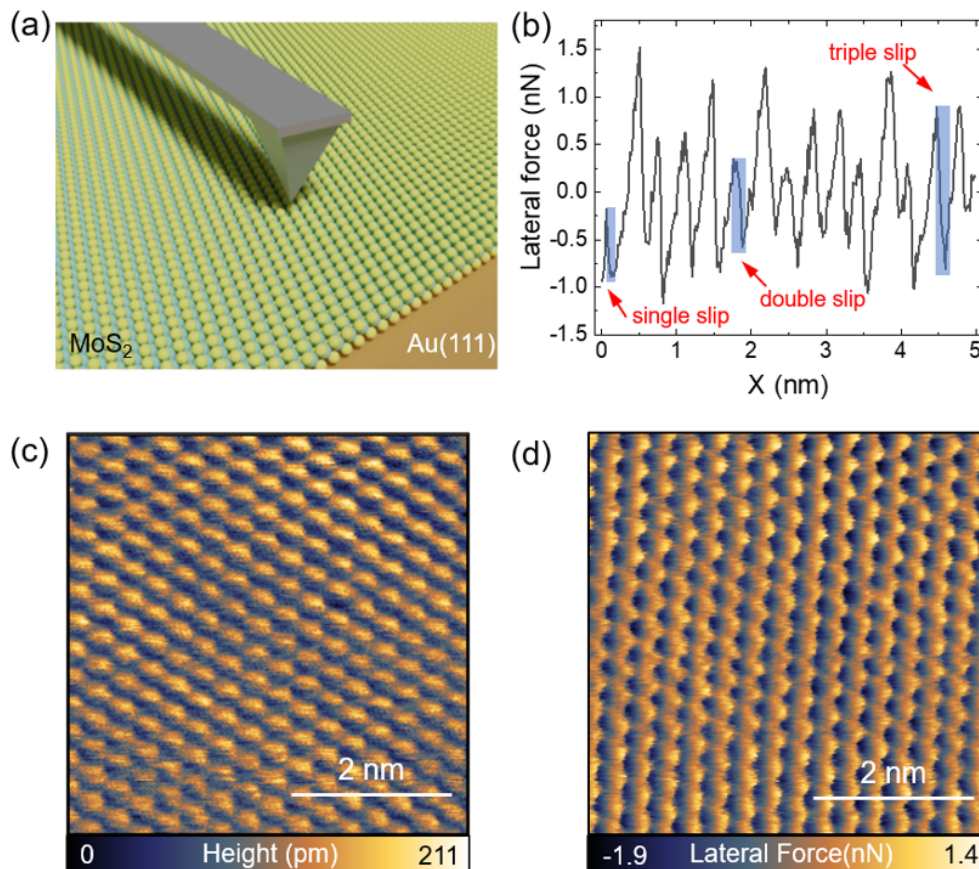friction, in quantitative agreement with experimental observations.

FIG. 1. **Experimental setup and atomic friction measurements of MoS$_2$.** (a) Schematic diagram of the experimental setup for measuring the friction between the sliding AFM tip and the MoS$_2$ layer. The MoS$_2$ was grown on the Au(111) substrate under UHV conditions. (b) Experimental lateral force trace showing different types of slips within one scan line. (c) Topography image and (d) corresponding lateral force obtained on the MoS$_2$ surface by AFM with atomic resolution. The hexagonal atomic structure of MoS$_2$ has a lattice constant of 0.31 nm. Measurement parameters: normal load $F_N = 1.1$ nN and sliding velocity $v = 195.3$ nm/s in (b), $F_N = 1.1$ nN and $v = 6.7$ nm/s in (c, d).

Experiments were performed with a silicon AFM tip sliding on monolayer MoS$_2$ grown under ultrahigh vacuum (UHV) conditions on a single crystal gold substrate. MoS$_2$ was prepared by Mo deposition on the freshly prepared Au(111) surface in H$_2$S atmosphere (the chamber pressure was kept at 1.0×10^{-6} mbar during the process) using an electron-beam evaporator. Subsequently, the sample was annealed at a temperature of 800 K, resulting in

the growth of single layer triangular MoS_2 flakes on the substrate [21]. Since the sample was grown and measured under UHV conditions, atomic cleanliness is preserved, which allows the acquisition of nanotribological properties of pristine MoS_2. The periodicity mismatch gives rise in our MoS_2/Au(111) system to a moiré structure with a periodicity of 3.3 nm [20, 22]. In some cases, the mechical properties such as stick-slip friction are influenced by the barrier arising when the tip crosses a boundary of the moiré patterns [23, 24]. However, in our MoS_2/Au(111) system, the strong interlayer interaction between sulfur layer and gold surface leads to the rigidity of the moiré corrugated MoS_2 surface [20, 25], so that no significant modulations from moiré pattern can be observed in the lateral force maps taken in contact mode (see Fig. 1(d)).

All measurements were performed using a home-built UHV AFM with beam deflection detection and running at a base pressure below 1×10^{-10} mbar and at room temperature. Fig. 1(a) illustrates the experimental setup. The normal spring constant of 0.2 N/m and the torsional spring constant of 125.5 N/m of a commercially available silicon cantilever (PPP-CONT, Nanosensors) are determined based on the geometrical parameters and the first resonance frequency of the cantilever (details are given in Supplemental Material). The normal and lateral forces acting on the tip were calibrated according to the methods described in Ref. [26]. The cantilever, before measurements, was annealed at $200\,^\circ$C for 1 h to remove the residual pollution on the tip and sputtered by Ar^+ ions for 2 min to remove the silicon dioxide covering the Si tip. The sliding velocity of AFM cantilever was primarily tuned by changing the scanning frequency. Figs. 1(c) and (d) show the topography and corresponding image of the lateral force measured on a monolayer MoS_2 in a range of 5×5 nm^2. The hexagonal atomic structure of the surface has a lattice constant of 0.31 nm.

The velocity-dependent experimental data of the friction force between the sliding AFM tip and the MoS_2 measured at different normal loads of $0.65, 2.0,$ and 2.5 nN are shown in Fig. 2. Three velocity regimes can be observed. A regular increase in friction at low velocities below a first transition velocity of 10 nm/s is followed by an abnormal decrease in friction up to a second transition velocity of about 100 nm/s and only then does an increase occur again. This non-monotonic velocity dependence of atomic friction is observed independently of different normal loads. The mechanically applied load through the tip apex, ranging from 0.65 to 2.5 nN, is in fact much smaller the adhesion force ≈ 19.9 nN between the AFM tip and the MoS_2 layer (see Supplemental Material), which dominates the effective load.
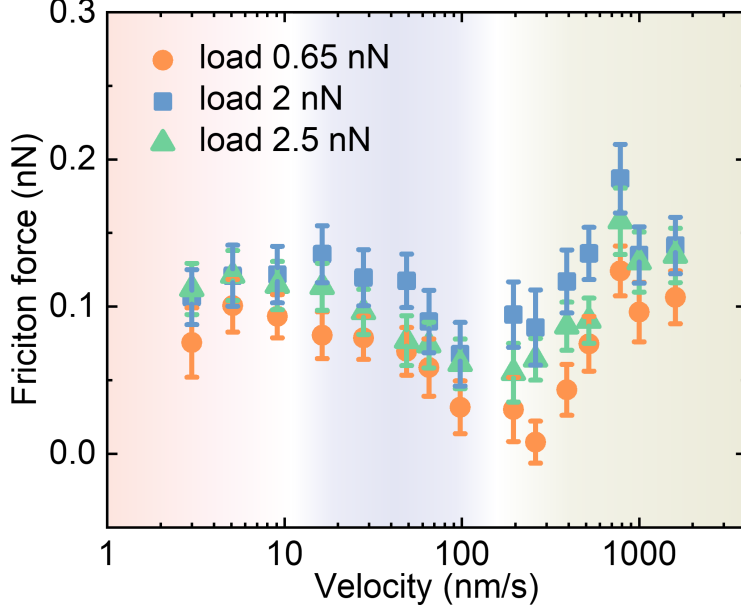
FIG. 2. Velocity dependence of the friction force between the sliding AFM tip and the MoS$_2$ surface measured at different normal loads of $0.65, 2.0,$ and $2.5\,\text{nN}$.

The gently increasing velocity dependence of atomic stick-slip friction in the first regime is readily understood. At high velocities there is less time for the thermal fluctuation to assist the tip apex to overcome the local energy barriers [9, 10, 13, 27, 28]. In the third, very high velocity regime, the stick-slip is suppressed, as indicated by the essentially linear friction growth. More interesting in our specific context is the non-monotonic decrease of friction in the second, intermediate regime.

To understand the non-monotonic velocity dependence of friction in the experiments, we conducted a theoretical study based on the thermally activated PT model. In the PT model the tip dynamics is given by [6, 7]:

$$m\ddot{x} = -\eta\dot{x} + \gamma(t) - \frac{\partial U^{\text{sub}}(x)}{\partial x} - \frac{\partial U^{\text{tip}}(x,t)}{\partial x} \qquad (1)$$

where m and x are the effective mass and the displacement of the tip, η is the damping coefficient, and γ is the thermal noise satisfying the fluctuation-dissipation relation, $\langle\gamma(t)\rangle = 0$ and $\langle\gamma(t)\gamma(0)\rangle = 2\eta k_{\text{B}}T\delta(t)$ [29]. The 3rd and 4th terms on the right-hand side are the forces due to the substrate corrugation and the cantilever $U^{\text{sub}}(x) = -\frac{U_0}{2}\cos(2\pi x/b)$ and $U^{\text{tip}}(x,t) = \frac{k_{\text{eff}}}{2}(vt-x)^2$, respectively. Here U_0 is the tip-surface energy barrier height, which is determined experimentally (see details in Supplemental Material), b is the substrate lattice
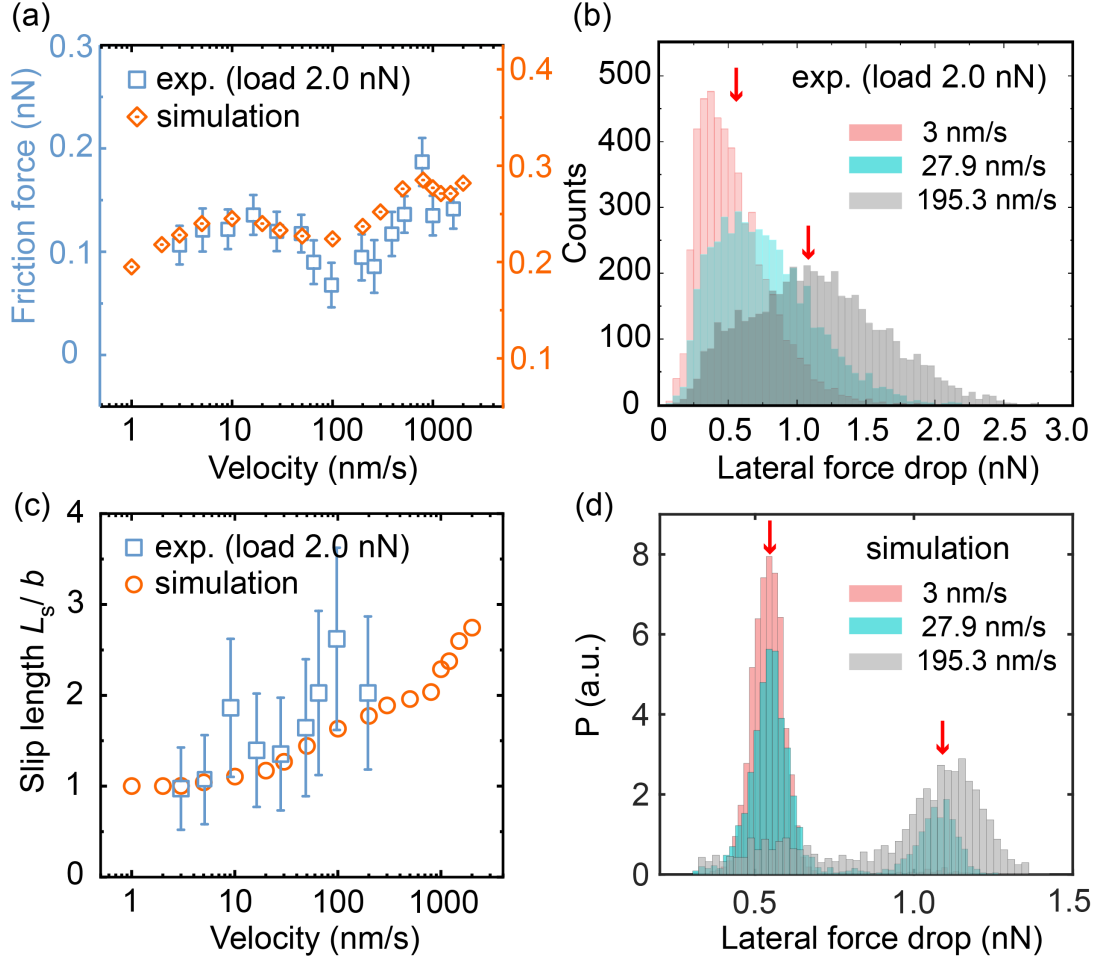
FIG. 3. (a) Non-monotonic frictional velocity dependence and the corresponding simulation result; (b) room temperature histograms of force drops obtained from experimentally measured lateral force traces for three typical velocities; (c) velocity dependence of the mean slip length L_s (normalized to lattice spacing b); (d) histograms of force drops obtained from simulated lateral force for three different velocities. The force drops corresponding to single slip and double slip are indicated by two red arrows in (b) and (d). Values of parameters used in simulations are: $U_0 = 0.44$ eV, $b = 0.315$ nm, $k_{eff} = 1.71$ N/m, $m = 2.84 \times 10^{-9}$ kg, $\eta = 3.32 \times 10^{-5}$ kg/s, and $T = 300$ K.

periodicity, k_{eff} is the effective lateral stiffness of the system, and v is the sliding velocity. The mean friction force F_k is extracted from the time-average of the steady-state lateral force. Using parameter values suggested from experiments, the simulation results for $F_k(v)$ show good agreement with the experiments (Fig. 3(a)). Beyond the important experimental velocity weakening, even subtle features, such as the small dip in the mean friction force at

$v \approx 1000$ nm/s are captured in the simulation.

Both experimental and simulated results show that the anomalous velocity weakening in the intermediate regime is due to a gradual change from single slip to multiple-slips as the velocity increases. The statistically obtained average slip length L_s (normalized to lattice spacing b) presented in Fig. 3(c), shows a clear increase above 1 with velocities between the first and second transition points. For single slips in each slip process, the tip jumps to the neighboring energy minimum, and the elastic energy stored in the stick period is released, with a drop of the lateral force $\Delta F_l = k_{eff} L_s$ (as shown in Fig. 1(b)). The evolution of this force with velocity and temperature is expected to lead to $F \sim (\ln v/T)^\gamma$, where γ is a positive exponent $2/3 < \gamma < 1$ [30, 31]. Fig. 3(b) presents a histogram of the force drops from the measured lateral force maps at three typical velocities 3, 27.9, and 195.3 nm/s, where at the low velocities, single and double slips were mainly revealed, whereas at higher velocities, genuine multiple-slips were detected (see Supplemental Materials for peak decomposition of these histograms). This is in agreement with the simulated results of Fig. 3(d), where histogram peaks are much narrower than for experimental data owing to a much smaller noise. The increase of L_s results in a larger drop of the lateral force during a slip, which in turn causes a drop of the time-averaged lateral force, i.e., the kinetic friction. From the perspective of energy dissipation, this F_k drop is attributed to the decrease of highly dissipative slip events, now rarefied with the increase in slip length. This explains the decrease in mean friction force seen in Fig. 3(a) at velocities from 10 to 100 nm/s and from 1000 to 1500 nm/s where the slip length increases significantly (Fig. 3 (c)), confirming the theoretical prediction. It is worth noting that although a similar non-monotonic dependence of F_k on velocity had been discussed theoretically [14–16], this is, to the best of our knowledge, the first time that this correlation has been observed experimentally in nanoscale tip/substrate systems. At the same time, the general agreement with the model-based PT simulations proves the accuracy of both our experimental and theoretical understanding.

Taking advantage of that, we can use simulations to gain a deeper fundamental understanding of the multiple-slips behavior and its velocity dependence beyond our experiments. We first generalize our simulation from a fixed surface corrugation energy $U_0 = 0.44$ eV to a wider range, from 0.2 to 1.0 eV, which are common values in other nanotribological experiments [8, 13, 32, 33]. A higher energy barrier should raise the static friction – the smallest lateral force to initiate the sliding, $F_s = \pi U_0/b$. Owing to a higher deformation

7

energy stored in the drag spring during the stick period, the tip should then have larger slip length, thus favouring multiple slips. As shown in Fig. 4, our simulations validate this expectation, both at 4(a) $T = 0$ and 4(b) $T = 300$ K (see also Supplemental Material).

In very low temperature and low velocity regimes where such details are more visible, the slip length L_s will be an integer multiple n of the lattice spacing b. From Ref. [18], the slip length nb occurs when $U_0 = E_n$, where $E_n = \frac{k_{\text{eff}} b^2}{2\pi^2 c_n}$, $c_n > 0$ being the slope of the n-th tangent ($y = \pm c_n x$) to the function $\sin x$. The first five values of c_n are 1, 0.217, 0.128, 0.0913 and 0.0709, which corresponds to the energies 0.0537, 0.247, 0.418, 0.588 and 0.758 eV. Except for the first level (0.0537 eV), which represents the transition from smooth sliding to stick-slip, the remaining four level are marked by red dashed lines in Fig. 4(a). They coincide quantitatively with the simulation results – the green-colored background of Fig. 4(a), which indicates a clear transition between multiple-slips.

At higher velocities, simulations show that the boundaries between different L_s regions bend down to smaller U_0. This is understood as a velocity assisted effect: the tip with higher kinetic energy crosses more efficiently the energy barrier. Therefore, for a fixed U_0, the slip magnitude tends to increase as velocity increases. This prediction agrees with both experiments and simulations, see Fig. 3(c). In other words, the barrier required to achieve the same slip length is reduced by kinetic energy [33, 34]. Based on the above understanding, the boundaries of different L_s regions, should be realistically represented by $E_n(v) = E_n - \frac{1}{2}mv^2$. As shown in Fig. 4(a), the red dashed lines based on this assumption agree well with simulation results.

At finite temperatures, thermal noise helps the tip to cross energy barriers. Therefore, achieving the same multiple-slips at finite temperature generally requires a larger energy barrier than at $T = 0\,\text{K}$. A series of simulations from 0 to $500\,\text{K}$ confirmed this expectation (Supplemental Material). Also due to thermal noise, the slip length no longer shows sharp boundaries, although smooth crossover boundaries can still be identified by the mean friction (see section 4 in Supplemental Material for more results under different temperatures). As already mentioned, any decrease in the mean friction force with increasing velocity means an increase in slip magnitude. Therefore, it is still possible to identify different regions of multiple-slips on the basis of the local maxima or plateaus of the mean friction. For a specific case, illustrated in Fig. 4(b), we simulated the dependence of friction upon velocity and corrugation magnitude at room temperature, and extracted the slip length in different
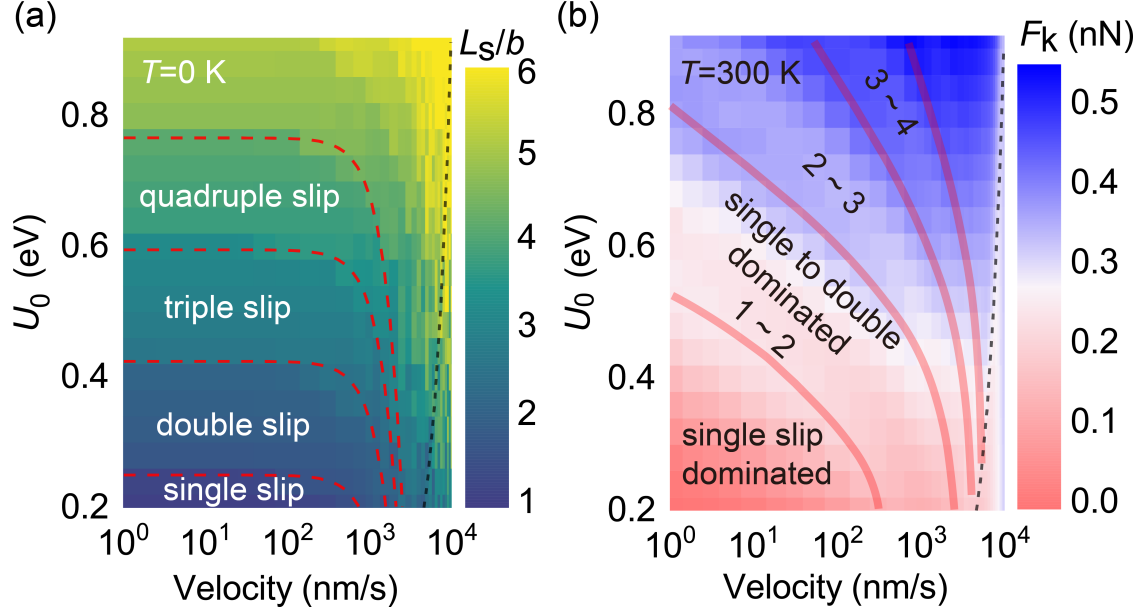
FIG. 4. (a) Phase diagram for the slip length L_{s} at $T = 0\,\mathrm{K}$. The red dashed lines indicate the boundary of different L_{s} regions, from deep green single slip region to light green multiple-slips regions. The frictional crossover "ridges" marked by red dashed lines coincide with the boundary of different slip length. (b) Dependence of the mean friction force on sliding velocity v and energy barrier U_0 at $T = 300$ K. Different friction regions indicated by the red shaded lines correspond to different slip length regimes, where L_s is no longer a constant. The black dotted line indicates the crossover from the stick-slip regime to a ballistic regime, which occurs when $U_0 \sim \frac{1}{2}mv^2$.

regions, and highlighted the local maximum of the mean friction force with red lines. As expected, these red lines coincide with the boundaries between different integer slip lengths. We found that the result shown in Fig. 3 is a special case with $U_0 = 0.44\,\mathrm{eV}$, and the non-monotonic $F_{\mathrm{k}}(v)$ relation corresponds to a horizontal section of the pattern in Fig. 4(b).

The elements determining the phase diagram of Fig. 4 also clarify the significance of the upper limiting velocity for multiple-slips. When the velocity is fast enough that the kinetic energy of the system becomes larger than the energy barrier, stick-slip disappears, the system enters the viscous dissipation regime. This upper limit is marked by the black dotted line in Figs 4(a) and (b) above which the velocity scaling of the mean friction becomes linear [35]. One thing to note in addition is that the damping coefficient η can influence the multiple-slips [17, 33, 36, 37], especially in the case of critical damping and overdamping $\eta \geq \eta_c = \frac{2\pi}{b}\sqrt{2U_0 m}$. We show in Supplemental Material additional simulation results of the

damping coefficient dependence of kinetic friction and slip length. The consistency between experiments and simulations of both friction force and slip length (Fig. 3) indicates that the underdamped regime is realistic in our case, consistent with the fact that sliding on the $MoS_2/Au(111)$ surface exhibits an ultra-low friction [20].

In summary, we reported the first experimental observation of non-monotonic velocity dependence of atomic friction caused by the onset of multiple-slips. The underlying phenomenology is explained in quantitative model simulations leading to a complete and more general stick-slip phase diagram with velocity-dependent boundaries between single, double, and multiple-slips. We expect that these results, revealing that multiple-slips can give rise to a substantial friction velocity weakening, should be of considerable importance in the broad field of nanotribology.

---

[1] C. M. Mate, G. M. McClelland, R. Erlandsson, and S. Chiang, Atomic-scale friction of a tungsten tip on a graphite surface, Phys Rev Lett **59**, 10.1103/PhysRevLett.59.1942 (1987).

[2] A. Socoliuc, R. Bennewitz, E. Gnecco, and E. Meyer, Transition from stick-slip to continuous sliding in atomic friction: entering a new regime of ultralow friction, Phys Rev Lett **92**, 10.1103/PhysRevLett.92.134301 (2004).

[3] X. Y. Zhao, S. R. Phillpot, W. G. Sawyer, S. B. Sinnott, and S. S. Perry, Transition from thermal to athermal friction under cryogenic conditions, Physical Review Letters **102**, 10.1103/PhysRevLett.102.186102 (2009).

[4] M. Urbakh and E. Meyer, Nanotribology: The renaissance of friction, Nat Mater **9**, 10.1038/nmat2599 (2010).

[5] E. Meyer, H. Hug, and R. Bennewitz, *Scanning Probe Microscopy: The Lab on a Tip* (Springer, 2021).

[6] L. Prandtl, Mind model of the kinetic theory of solid bodies, Zeitschrift Fur Angewandte Mathematik Und Mechanik **8**, 85 (1928).

[7] G. A. Tomlinson, A molecular theory of friction, Philosophical Magazine **7** (1929).

[8] E. Gnecco, R. Bennewitz, T. Gyalog, C. Loppacher, M. Bammerlin, E. Meyer, and H. Guntherodt, Velocity dependence of atomic friction, Phys Rev Lett **84**, 10.1103/PhysRevLett.84.1172 (2000).

[9] E. Riedo, E. Gnecco, R. Bennewitz, E. Meyer, and H. Brune, Interaction potential and hopping dynamics governing sliding friction, Phys Rev Lett **91**, 10.1103/PhysRevLett.91.084502 (2003).

[10] Q. Li, Y. Dong, D. Perez, A. Martini, and R. W. Carpick, Speed dependence of atomic stick-slip friction in optimally matched experiments and molecular dynamics simulations, Phys Rev Lett **106**, 10.1103/PhysRevLett.106.126101 (2011).

[11] X. Z. Liu, Z. Ye, Y. Dong, P. Egberts, R. W. Carpick, and A. Martini, Dynamics of atomic stick-slip friction examined with atomic force microscopy and atomistic simulations at overlapping speeds, Phys Rev Lett **114**, 10.1103/PhysRevLett.114.146102 (2015).

[12] O. Acikgoz and M. Z. Baykara, Speed dependence of friction on single-layer and bulk mos2 measured by atomic force microscopy, Applied Physics Letters **116**, 10.1063/1.5142712 (2020).

[13] A. Vanossi, N. Manini, M. Urbakh, S. Zapperi, and E. Tosatti, Colloquium: Modeling friction: From nanoscale to mesoscale, Rev. Mod. Phys. **85**, 10.1103/RevModPhys.85.529 (2013).

[14] Z. Tshiprut, S. Zelner, and M. Urbakh, Temperature-induced enhancement of nanoscale friction, Physical Review Letters **102**, 10.1103/PhysRevLett.102.136102 (2009).

[15] P. Reimann and M. Evstigneev, Nonmonotonic velocity dependence of atomic friction, Phys Rev Lett **93**, 10.1103/PhysRevLett.93.230802 (2004).

[16] J. Nakamura, S. Wakunami, and A. Natori, Double-slip mechanism in atomic-scale friction: Tomlinson model at finite temperatures, Physical Review B **72**, 10.1103/PhysRevB.72.235415 (2005).

[17] R. Roth, T. Glatzel, P. Steiner, E. Gnecco, A. Baratoff, and E. Meyer, Multiple slips in

atomic-scale friction: An indicator for the lateral contact damping, Tribology Letters **39**, 10.1007/s11249-009-9567-7 (2010).

[18] S. N. Medyanik, W. K. Liu, I. H. Sung, and R. W. Carpick, Predictions and observations of multiple slip modes in atomic-scale friction, Physical Review Letters **97**, 10.1103/PhysRevLett.97.136106 (2006).

[19] J. M. Martin, C. Donnet, T. Le Mogne, and T. Epicier, Superlubricity of molybdenum disulphide, Phys Rev B Condens Matter **48**, 10583 (1993).

[20] Y. Song, A. Hinaut, S. Scherb, Y. Pellmont, R. Pawlak, S. Huang, Z. Liu, T. Glatzel, and E. Meyer, Observation of robust superlubricity of mos2 on au (111) in ultrahigh vacuum, Appl Surf Sci **601**, 10.1016/j.apsusc.2022.154230 (2022).

[21] S. G. Sorensen, H. G. Fuchtbauer, A. K. Tuxen, A. S. Walton, and J. V. Lauritsen, Structure and electronic properties of in situ synthesized single-layer mos2 on a gold surface, Acs Nano **8**, 6788 (2014).

[22] N. Krane, C. Lotze, J. M. Lager, G. Reecht, and K. J. Franke, Electronic structure and luminescence of quasi-freestanding mos2 nanopatches on au(111), Nano Letters **16**, 5163 (2016).

[23] S. Zhang, Q. Yao, L. Chen, C. Jiang, T. Ma, H. Wang, X.-Q. Feng, and Q. Li, Dual-scale stick-slip friction on graphene/h-BN moiré superlattice structure, Physical Review Letters **128**, 226101 (2022).

[24] Y. M. Song, X. Gao, A. Hinaut, S. Scherb, S. Y. Huang, T. Glatzel, O. Hod, M. Urbakh, and E. Meyer, Velocity dependence of moire friction, Nano Letters **22**, 9529 (2022).

[25] C. C. Silva, D. Dombrowski, N. Atodiresei, W. Jolie, F. F. zum Hagen, J. Q. Cai, P. T. P. Ryan, P. K. Thakur, V. Caciuc, S. Blugel, D. A. Duncan, T. Michely, T. L. Lee, and C. Busse, Spatial variation of geometry, binding, and electronic properties in the moire superstructure of mos2 on au(111), 2d Materials **9**, 10.1088/2053-1583/ac4958 (2022).

[26] E. Gnecco and E. Meyer, *Fundamentals of Friction and Wear on the Nanoscale* (Springer, 2015).

[27] K. B. Jinesh, S. Y. Krylov, H. Valk, M. Dienwiebel, and J. W. M. Frenken, Thermolubricity in atomic-scale friction, Physical Review B **78**, 10.1103/PhysRevB.78.155440 (2008).

[28] L. Jansen, H. Holscher, H. Fuchs, and A. Schirmeisen, Temperature dependence of atomic-scale stick-slip friction, Physical Review Letters **104**, 10.1103/PhysRevLett.104.256101 (2010).

[29] R. Kubo, The fluctuation-dissipation theorem, Reports on Progress in Physics **29**, 255 (1966).

[30] Y. Sang, M. Dube, and M. Grant, Thermal effects on atomic friction, Physical Review Letters **87**, 10.1103/PhysRevLett.87.174301 (2001).

[31] M. H. Müser, Velocity dependence of kinetic friction in the prandtl-tomlinson model, Phys. Rev. B **84**, 125419 (2011).

[32] M. Dienwiebel, G. S. Verhoeven, N. Pradeep, J. W. Frenken, J. A. Heimberg, and H. W. Zandbergen, Superlubricity of graphite, Phys Rev Lett **92**, 10.1103/PhysRevLett.92.126101 (2004).

[33] Y. Dong, A. Vadakkepatt, and A. Martini, Analytical models for atomic friction, Tribology Letters **44**, 10.1007/s11249-011-9850-2 (2011).

[34] Y. L. Dong, D. Perez, A. F. Voter, and A. Martini, The roles of statics and dynamics in determining transitions between atomic friction regimes, Tribology Letters **42**, 99 (2011).

[35] S. Y. Krylov and J. W. M. Frenken, The physics of atomic-scale friction: Basic considerations and open questions, physica status solidi (b) **251**, 711 (2014).

[36] E. Gnecco, R. Roth, and A. Baratoff, Analytical expressions for the kinetic friction in the prandtl-tomlinson model, Phys. Rev. B **86**, 10.1103/PhysRevB.86.035443 (2012).

[37] E. Gnecco, L. Agmon, and R. Berkovich, Friction and chaos: Influence of the damping co-efficient on atomic-scale stick-slip on hexagonal crystal lattices, Phys. Rev. B **105**, 235427 (2022).